Numerical investigation of EDZ development around a deep polymetallic ore mine

Mountaka Souley, Marwan Al Heib, Vincent Renaud

Numerical investigation of EDZ development around a deep polymetallic ore mine

Mountaka Souley [a]*, Marwan Al Heib [a], Vincent Renaud [a]

[a] INERIS, c/o Ecole des Mines de Nancy, Campus ARTEM, CS 14234, Nancy, France, F-54042

ABSTRACT
This paper deals with the development of a non-linear constitutive model of rock mass and its verification to predict a damaged zone. Simulations of triaxial compressions provide a verification of the implementation with a good agreement between predictions and theoretical values of peak and residual strengths as well as the transition between brittle failure and ductile response. The applicability of the model to predict potential failure around stopes of a deep polymetallic ore mine is checked. The present study highlights the interest to consider more realistic rheology of hard rock masses compared with the elastic perfectly plastic models of underground deep mines.
KEYWORDS: Brittle-ductile behaviour; constitutive model; verification; Garpenberg mine; numerical modelling

1. INTRODUCTION

Damage by microcracking is the main dissipation process associated with inelastic behaviour and failure in most brittle materials such as rocks, concrete and ceramic composites. Under high *in situ* and induced stresses and high anisotropic stress ratios, an excavation damaged zone (EDZ) may be formed around underground openings excavated into brittle rocks. The failure mechanism in this damaged zone is the initiation, growth and coalescence of cracks and fractures and is directly related to the constitutive behaviour of rock mass. Experimental studies on brittle rocks have shown that there are many different mechanisms by which cracks can be initiated and grown under compressive stresses (Steif, 1984; Horii and Nemat-Nasser, 1986,). The involved mechanisms include sliding along pre-existing cracks and grain boundaries, pore crushing, elastic mismatch between mineral grains and dislocation movement, etc. Indeed, irreversible deformations and failure of rocks subjected to stresses occur through progressive damage as micro-cracks initiate and grow at small scale and coalesce to form large-scale fractures and faults. Over the past decade, several constitutive models have been developed providing a more realistic description of damage for brittle rocks in relation to experimental observations (Zhu et al. 2009).

In the framework of the European program I_2Mine (http://www.i2mine.eu/), INERIS has developed an innovative tool (stress monitoring tool) aimed to better understand the behaviour of the rock mass resulting from the mining process of Garpenberg deep mine (superposed rooms and pillars and vertical stopes between depths 1100 and 1300 m, Figure 1) in Sweden. Several seismic sensors and strain gauges were installed in a deep area of the mine (approximately at 1150 m deep) to monitor the evolution of induced stresses during the exploitation and the related induced seismic activities.

The objective of this paper is to study the mechanical behaviour of the main galleries and the pillars by incorporating the stages of the underground work through advancing numerical modelling. At first approach, we are limited to 2D models that take into account the initial state of stress (anisotropic) and the mine operations.

More precisely, the purpose of this paper is to present: (a) a numerical implementation of an elastoplastic model obeying to the Hoek–Brown criterion and taking into account the brittle/ductile transition between the brittle failure and the ductile behaviour depending on the mean stress as generally observed on most rock samples: that is to say, the initiation and growth of cracks for brittle rocks are modeled by a softening behaviour in the post-peak in the framework of plasticity theory, (b) the corresponding verification based on simulation of triaxial compression tests. Finally, the numerical modelling provides the localization of EDZ and the potential instability area in the vicinity of stopes located around the pilot area of the mine works at the Garpenberg mine (New Boliden company).

2. PROPOSED RHEOLOGICAL MODEL AND NUMERICAL IMPLEMENTATION

The mechanical behaviour of geomaterials is widely varied and depends mainly on the confining stress (or mean stress) and the loading paths. At low stress confining levels, rocks break by the creation of

*Corresponding author – email: Mountaka.Souley@ineris.fr

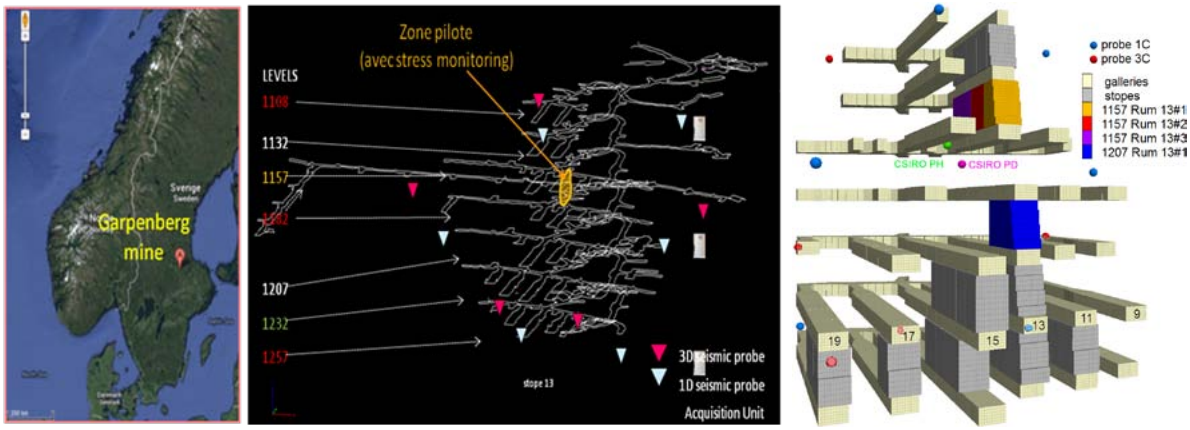

Figure 1: Experimental set-up (stress and microseismic measurements) in the Swedish mine Garpenberg: (a-left) the mine location; (b-centre) operating plan and location of the pilot area; (c-right) 3D mesh of galleries and stopes.

one or more shear planes or bands accompanied by a strain-softening behaviour characterized by microcracks dilatancy and grains rotation at the microscopic scale. Under high mean stresses, rocks undergo a hardening behaviour which is microscopically associated with volumetric strains. More precisely, for most geomaterials subjected to triaxial compressions under low to moderate confining pressures, it is generally observed the following typical characteristics of stress-strain curves: (a) a linear isotropic and elastic behaviour after a short non-linear phase corresponding to the closure of the initial pores and the progressive contact walls of the original micropores and microcracks (b) a strain-hardening in the pre-peak region corresponding to the initiation and the growth of microcracks modeled generally by the plasticity theory or the damage mechanics through the concept of effective stress and the hypothesis of strain equivalence (c) a strain-softening after reaching the peak strength (failure) associated with a progressive loss in material cohesion and then a decrease in strength (d) a phase where the rock strength remains practically constant. Relative to the elasto-brittle materials where the initial microcracks closure and the growth of microcracks in the pre-peak domain can be neglected in a first approximation (as it is the typical case of hard rock masses studied herein at the Garpenberg mine), the present study considers an isotropic elastic linear behaviour before the peak.

The Hoek-Brown criterion widely used in the field of rock mechanics and rock engineering, whose limitations were documented by detailed discussions of the simplifying assumptions (Hoek and Brown, 1980), was generalized in terms of the three stress invariants in this study. One of the most important limitations is the non-dependency of the criterion on the intermediate principal stress, σ_2. Subsequent experimental studies have since suggested that the intermediate principal stress has a substantial influence on the rock strength (e.g. Haimson, 2006). This has led to the development of several 3D versions of the Hoek–Brown failure criterion (Priest, 2005; Zhang, 2008).

It is well known that the three principal stresses σ_1, σ_2 and σ_3 can alternatively be expressed in terms of mean stress (p), generalized deviatoric stress (q) and Lode's angle (θ) and vice versa, which allows to express the classical Hoek-Brown criterion in 3D-stresses space (p, q, θ). After some manipulations, the generalized yield function is proposed on the basis of Souley et al. (2011):

$$F_s = \frac{4\cos^2\theta}{3\sigma_c} q^2 - m\left(\frac{\cos\theta}{\sqrt{3}} - \frac{\sin\theta}{3}\right) q + m\,p - s\sigma_c \quad (1)$$

where σ_c is the uniaxial compressive strength of the intact rock, m, s represents the rheological behaviour parameters whose significance and quantification differ from the dimensionless empirical parameters of Hoek-Brown reflecting the strength of the intact rock, the natural fractured rock mass and therefore consideration of a possible scale effect and fracturing at the large scale. The parameter m quantifies the frictional strength and s (measuring the induced cracks) is related to the rock cohesion.

Let (m_p, s_p) and (m_r, s_r) be respectively the values of parameters (m, s) at the peak and the beginning residual phase. Assuming a transition between brittle and ductile behaviour, equation (1) makes it possible to express a relationship between the peak and residual strength parameters:

$$m_r = m_p + (s_p - s_r)\frac{\sigma_c}{{\sigma_3}^{b-d}} \quad (2)$$

In the absence of experimental data on the residual strength, almost null value of s_r can be considered as a good approximation in relation to

sliding along the macroscopic failure planes or shear bands. For softening phase, the same yield function (equation 1) is used by introducing the softening internal variable (ξ). In accordance with the yield function used, (a) the generalized plastic strain is chosen to represent the internal variable, (b) m linearly varies with ξ between the peak and the beginning of residual phase ($0 < \xi \leq \xi_r$ representing the shear plastic strain) whereas s varies non linearly (c) m and s remain constant in the residual domain:

$$d\xi = \sqrt{\frac{2}{3} d\underline{e}^p : d\underline{e}^p} \qquad m = m_p + (m_r - m_p)\frac{\xi}{\xi_r} \quad (3)$$

$$s = s_p + (s_r - s_p)\left(2 - \frac{\xi}{\xi_r}\right)\frac{\xi}{\xi_r} \quad (4)$$

where $d\underline{e}^p$ is the increment of deviatoric plastic strain tensor in post-peak or residual regions.

Assuming for this type of rock materials that the plastic dilatancy occurs only near the peak strength and cannot exceed a threshold rate (β_m) for a certain value of deformation and by adapting a non associated flow rule (generally accepted for rock materials), we propose the following plastic potential (G_s) which allows to express the constitutive relationship between the increments of stresses ($d\underline{\sigma}$) and total strains as follows ($d\underline{\varepsilon}$):

$$G_s = q - \beta_m(1 - e^{-b_1 \xi})p \quad (5)$$

$$d\underline{\sigma} = \left[\underline{\underline{C}} - \frac{\left(\underline{\underline{C}} : \frac{\partial F_s}{\partial \underline{\sigma}}\right) \otimes \left(\underline{\underline{C}} : \frac{\partial F_s}{\partial \underline{\sigma}}\right)}{\frac{\partial F_s}{\partial \underline{\sigma}} : \underline{\underline{C}} : \frac{\partial G_s}{\partial \underline{\sigma}} - \frac{\partial F_s}{\partial \xi}\frac{\partial G_s}{\partial q}}\right] d\underline{\varepsilon} \quad (6)$$

In addition to the two elastic constants: Young modulus and Poisson ratio (E, ν), the needed parameters for the proposed model are: m_p, m_r, $\sigma_3^{b\text{-}d}$, s_p, s_r, σ_c, ξ_r, β_m and b_1. All of these parameters can be identifiable from triaxial compression tests (3 minimum) carried out from low confining pressure (or without) to high confining pressure (characterizing $\sigma_3^{b\text{-}d}$). Finally the proposed model was implemented in the three-dimensional explicit finite-difference code, *FLAC*^{3D}, where a perfect elastoplastic model with the Hoek-Brown criterion in the (σ_1, σ_3) plane already exists in the commercial version.

The most input data used in this paper are from laboratory tests, field studies, reports and papers. More precisely, the Young's modulus (E), Poisson's ratio (ν) and the unconfined compressive strength (σ_c) have been obtained from the point and biaxial load tests or uniaxial compression loading carried out on samples (complex ores containing zinc, lead, silver, copper and gold) taken from the measuring holes at -883 m and -967 m levels (Edelbro, 2008; van Koppen, 2008). These parameters and the empirical constants m_p and s_p, and dilatancy at failure were confirmed by many numerical studies aimed to the calibration of the mechanical characteristics, the determination of the in situ stresses (at -880 m level and from one access gallery at -1155 m level, respectively carried out by Boliden and INERIS) and the understanding of the failure mechanism (for instance spalling, shear failure, slabbing, buckling or other types of compressive failure) as well as the back-evaluation of fallout extent observed in the field.

It is known that it is often very difficult to get the full stress-strain curves of the post-peak behaviour particularly for hard rock masses exhibiting brittle behaviour. As first approach, we retained the values of additional parameters (s_r, $\sigma_3^{b\text{-}d}$, ξ_r, β_m and b_1) summarized in Table 1: a sensitivity analysis on these parameters will be conducted in parallel to the interpretation of the in situ stress measurements at 1155 m coming in the future and whose deformation measurement systems have already been installed from an access gallery at -1155 m level (Figure 1c).

Table 1: Numerical values of input model parameters.

Parameter	Value	Parameter	Value
E (MPa)	80000	s_r (-)	10^{-5} s_p
ν	0.2	$\sigma_3^{b\text{-}d}$ (MPa)	$\sigma_c \sqrt{s} \approx 63$
m_p (-)	10	ξ_r (-)	0.0025
s_p (-)	0.112	β_m(-)	tan(15°)
σ_c (MPa)	188	b_1(-)	750

3. NUMERICAL IMPLEMENTATION AND MODEL VERIFICATIONS

In order to verify the implemented model, seven triaxial compression tests with confining pressures ranged from 0.01 to 75 MPa have been simulated. The input parameters used for this exercise are summarized in Table 1.

Figure 2 presents the deviatoric stress versus axial and lateral strains curves for different confining pressure (σ_3). We note that the post-peak behaviour is confining pressure dependent: the transition stress between brittle failure and ductile behaviour is clearly marked and the numerical transition stress, $\sigma_3^{b\text{-}d}$, occurs for a confining pressure of 63 MPa in accordance with the input numerical value.

Figure 3 shows a comparison in terms of the peak and residual strengths between the predictions and theoretical expression in equation (1) (with $\theta = 30°$ for triaxial compression loading path). The match is very good as may be seen in this figure, where numerical and analytical solutions coincide.

The relative error for peak and residual strengths is less than 0.3 % and 0.7 % respectively for peak and residual strengths. This validates the numerical implementation of the proposed elastoplastic model in *FLAC*^{3D}.

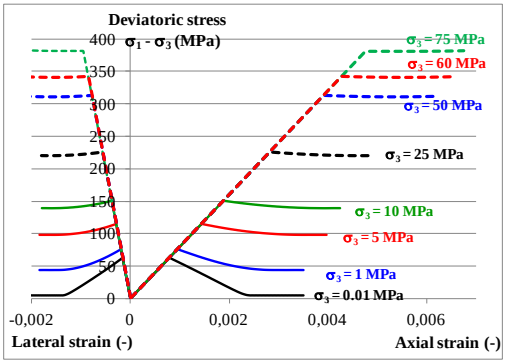

Figure 2: Numerical results of triaxial compression tests.

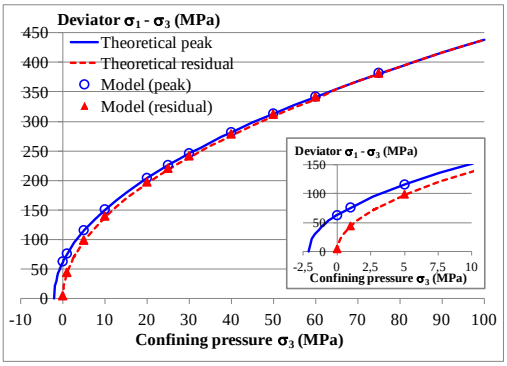

Figure 3: Peak and residual strengths: numerical and analytical solutions.

4. APPLICATION TO GARPENBERG MINE

The aim of this section is to provide a verification of the implementation for non-triaxial stress paths and to show numerically the ability of the model to evaluate the extent of potential damaged zones in relation to the excavation of one or more stopes.

In the Garpenberg mine, polymetallic ore is extracted which contains zinc, silver, lead, copper and gold. The ore has fold axis and the depth is 500-1300 m below the surface. During the mining operations of the upper level (-883 m and -967 m levels), several field studies and numerical modellings were performed with the aim to calibrate certain mechanical characteristics, back-determine the initial and induced *in situ* stresses and to understand the potential failure mechanisms. The results of these observations and measurements were also used as input data for the preliminary 3D modelling of the initial stress field prevailing at the lower level around 1155 m deep before the future excavation of stopes and for which stress measurements are available using CSIRO cells (Figure 4).

To retrieve the initial stress state (at 1155 m), a 3D numerical model has been carried out with several assumptions. A specific methodology for verifying the correlation of measured stresses (where locations are illustrated in Figure 4) with computed stresses (after mining operations of the upper level) is developed: it consists of creating a stress data bank with the numerical model according to the range of measured stress tensors. Because the dependence between initial and induced stresses is strongly non-linear, it is very difficult to find what is the initial stress tensor that produces the correct measured stresses after the excavation of many galleries and stopes and after a partial backfilling of the stopes (chambers). Nevertheless, it was possible to estimate the initial stress tensor corresponding to level -1155 m. The horizontal and vertical directions are principal with the following principal values 47.5 MPa (x-horizontal direction), 55 MPa (y-horizontal direction) and 20.5 MPa (vertically). This stress state was used to uniformly load the numerical 2D-model shown in Figure 4.

As illustrated in Figure 1c, to model the mine geometry in 2D as first stage, we can consider a double symmetry in the vertical and horizontal directions. The geometrical model for 2D-modelling with *FLAC*^{3D} assuming plane strain conditions is shown in Figure 4. Null normal displacements are imposed at the boundary limits (symmetry). The access galleries are 10 m wide and 6 m high. Finally, typical primary stope sizes are: 80 m long (along Y-direction), 10 m wide, and 19 m high.

The modelling sequences were performed as follows: (a) model without excavations was consolidated under the previous initial in situ stresses, using roller boundaries to the model sides respectively parallel to x- and z-axis for seeking symmetry (step 0); (b) four galleries are simultaneously excavated, numerical model is stepped until equilibrium (step 1) and (c) stopes 1 and 2 are simultaneously deleted and the numerical model is stepped until equilibrium.

The plastic zones corresponding to the galleries excavation (phase 1) (or failed with behaviour in residual or transition between peak and residual) are limited to the galleries skin. This is consistent with the observed fallouts (whose extension is around 0.05 m) or predicted by numerical analysis conducted at -880 m level. This is also consistent with the strength of the rock masses ($\sigma_c\sqrt{s}\approx 63$ MPa) and the magnitude of induced stresses. In considering for example the case of the gallery sides and assuming the linear elasticity behaviour and neglecting variations of axial stress, the expected orthoradial, radial, and axial

stresses are globally 16, 0, and 50 MPa. This confirms the failure at the walls. Moreover, away from the wall, the presence of a non null radial stress significantly increases the rock mass strength by the term ($m_p\sigma_r\sigma_c$), which explains the limited character of failed area around the galleries.

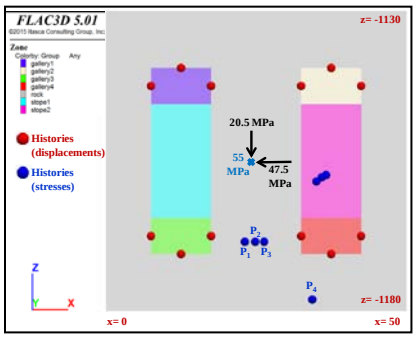

Figure 4: Geometrical model with position of history points.

After excavating the two stopes in a 2D model, the extent of plastic zones is concentrated in the pillar (Figure 5), in the compressive region where the maximum deviatoric stress is located (at the heart of pillars between stopes along the symmetry axis). Figure 5a shows the distribution of plastic zones in the pillars (and therefore strain localization). In fact, the most compressive stresses are located at the singularity levels (corners of galleries), but as the mean stress also increases in magnitude, it is the same for the failure strength. Excavation of stopes results in complete release of the horizontal stress, causing predominantly tensile stresses over the whole width and substantially all the height of pillars. Therefore, the failures can be initiated at the center of pillars and propagate along an inclined plane at first and then sub-vertically following the localization of the plastic zones. As a consequence of stress projections on the current yield envelop, we observed decreases in the vertical and axial stresses. This is well illustrated in Figure 6, which shows the distribution of horizontal and vertical stresses at the end of step 2.

For comparison purpose and in order to capture the contribution of the proposed rheological model (#1), another simulation is performed with a basic perfectly plastic model with Hoek-Brown's criterion (model #2). In this case, the plastic zones are also developed in the heart of the pillars but in a very limited area compared to the results of the model #1 (previously presented) without plastic strain localization (Figure 5b). Specifically, the examination of the principal stresses (σ_1, σ_2, σ_3) at the pillar center delimited by the two stopes for the two models 1 and 2 provides the following stress values: (-20.5, -17.5, 0.75 MPa) and (-48, -35.5, 0.85 MPa) respectively for #1 and #2 (compressive stresses < 0). Finally, Figure 6b clearly shows a significant increase in vertical stress (σ_{zz}) near the changes of orientations of failure plane locations, indicating some eventual seats of potential risks of instability.

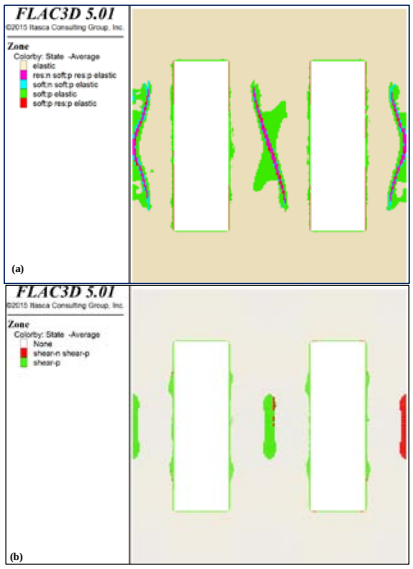

Figure 5: Extent of plastic zones around the stopes: (a) model #1 (b) model #2.

The quantitative comparison between the two models was conducted on the stress values at the end of step 2 (points 1 to 4 illustrated in Figure 4) and reported in Table 1 in terms of stress ratios with respect to the initial stress state before the excavations of galleries and stopes.

One can note that in both cases, the four points are outside the plastic domain induced by galleries and stopes. The points P_1, P_2, and P_3 are located in the pillar between the two lower galleries and point P_4 is located at the floor of a stope. Table 2 reveals a slight difference between the models on the relaxation at P_1, P_2, and P_3 and compression at P4 of the horizontal stresses (along x and perpendicular to the model cross section). Conversely, over-stresses develop in the vertical direction at P_1, P_2, and P_3 positions with more magnitude (15 to 35%) for #1 compared to #2, resulting from the failure occurred a little earlier in the pillar of stopes, and then a new stresses redistribution.

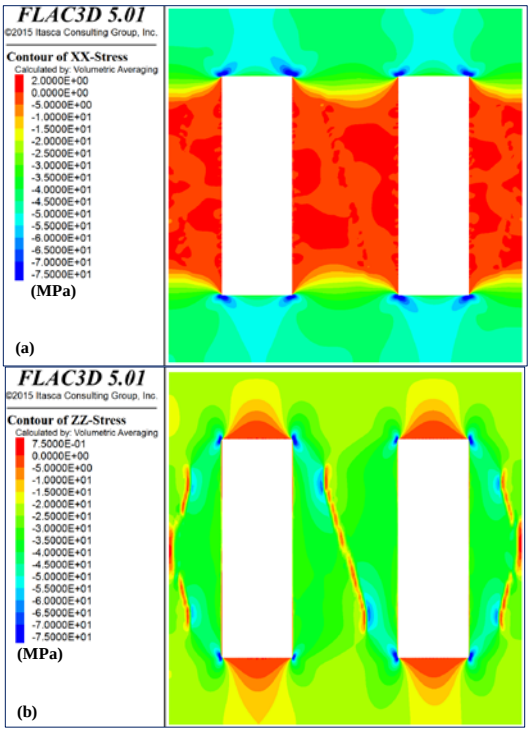

Figure 6: Horizontal (top) and vertical (down) stresses: model #1.

Table 2: Ratio of horizontal (σ_{xx}), vertical (σ_{zz}) and axial (σ_{yy}) stresses.

Model	σ_{xx}^{*} P_1	σ_{zz}^{*} P_1	σ_{yy}^{*} P_1
#1	0.38	1.45	0.93
#2	0.41	1.59	0.94
Model	σ_{xx}^{*} P_2	σ_{zz}^{*} P_2	σ_{yy}^{*} P_2
#1	0.39	1.31	0.92
#2	0.42	1.57	0.94
Model	σ_{xx}^{*} P_3	σ_{zz}^{*} P_3	σ_{yy}^{*} P_3
#1	0.41	1.22	0.91
#2	0.41	1.58	0.94
Model	σ_{xx}^{*} P_4	σ_{zz}^{*} P_4	σ_{yy}^{*} P_4
#1	1.04	0.96	1
#2	1.05	0.87	1

5. CONCLUSION

This paper presents the development of a constitutive model for brittle hard rock masses, its numerical implementation in the three-dimensional code *FLAC*^{3D}, as well as its verification. Simulation of triaxial compression tests at different levels of confining pressure provides a verification of the implemented model. The resulting curves display three regions (elastic, softening in post-peak, and residual phase) as well as a transition between brittle failure and ductile behaviour as generally observed on hard and brittle rocks. The ability of the proposed model to predict the potential failure regions (damaged zones) around deep underground excavations in hard rocks is successfully tested. In particular, the importance of considering the post-peak behaviour to predict strains and failure zones localization, and consequently the advantage over the approaches without strain softening is shown.

It is often difficult to characterize the post-peak behaviour parameters from laboratory tests on such hard rocks in relation to the brittle nature of their behaviour. These parameters can be viewed as calibration parameters, which can be back-determined on the base of the in situ observations. The prospect of this work after a full 3D modelling back-analysis would complete this numerical development by implementing the energy balance in view of assessing the proneness to rockbursts or strain bursts.

6. REFERENCES

Edelbro C. (2008). Strength, fallouts and numerical modeling of hard rock masses. Doctoral thesis 2008:56, Lulea University of Technology, 80p.

Haimson B. (2006). True triaxial stresses and the brittle fracture of rock. Pure Applied Geophysics. Volume 163(5–6), pp. 1101–1130.

Hoek E. and Brown ET. (1980). Underground excavations in rock. The Institution of Mining and Metallurgy, London.

Horii H. and Nemat-Nasser S. (1986). Brittle failure in compression: splitting, faulting and brittle-ductile transition. Philos. Trans. R. Soc. (London), Series A, Vol. 319, pp. 337-374.

Priest S.D. (2005). Determination of shear strength and three-dimensional yield strength for the Hoek–Brown criterion. Rock Mechanics and Rock Engineering. Vol. 38(4), pp. 299–327.

Souley M., Armand G., Su K. and Ghoreychi M., (2011). Modelling of the viscoplastic behaviour including damage for deep argillaceous rocks, Physics and Chemistry of the Earth, 36, pp. 1949–1959.

Steif P.S. (1984). Crack extension under compressive loading. Engineering Fracture Mechanics. Volume 20(3), pp. 463-473.

van Koppen M.J.G. (2008). Estimation of the Risk for Mine Induced Seismicity in Large Scale Mining in the Garpenberg Mine. Master of Science, Delft University of Technology, Netherlands.

Zhang L. (2008). A generalized three-dimensional Hoek–Brown strength criterion. Rock Mechanics and Rock Engineering. Vol.41(6), pp. 893–915.

Zhu Q.Z., Kondo D. and Shao J.F. (2009). Homogenization-based analysis of anisotropic damage in brittle materials with unilateral effect and interactions between microcracks. Int J of Num and Anal Methods in Geomech. Vol. 33, pp. 749–72.